Weather and Climate Extremes 19 (2018) 20–28

Contents lists available at ScienceDirect

Weather and Climate Extremes

journal homepage: www.elsevier.com/locate/wace

Extreme temperature differences in the city of Lahti, southern Finland: Intensity, seasonality and environmental drivers

Juuso Suomi

Department of Geography and Geology, University of Turku, FI-20014, Turku, Finland

ARTICLE INFO

Keywords:
Extreme temperature difference
Land use
Topography
Urban heat island
Water body
Seasonality

ABSTRACT

The extremes of month-specific spatial temperature differences were studied for a first time in the high-latitude city of Lahti and its surroundings in southern Finland. During the 2-year observation period (6/14–5/16), the largest momentary temperature difference, 11.1 °C, was detected in February, and the smallest, 6.2 °C, in April. The impacts of various environmental factors during the extreme situations were estimated by site-specific analysis of the warmest and coldest observation sites and a stepwise multiple linear regression model including all the 8 observation sites. The extreme temperature differences were characterised by inversions especially in winter and spring, the warmest site being the hill-top location in Kivistönmäki. In summer the role of urban heating was more apparent, and the temperature was the highest in the relatively low-lying city centre. In autumn the heating impact of the relatively warm Lake Vesijärvi caused the largest temperature differences with harbour as the warmest site. The weather during all of the momentary extreme situations was calm and in the majority of the situations also clear. The impact of cloud cover was less critical than that of wind speed in reducing spatial temperature differences. The momentary extreme situations existed at night or at dawn, with one exception: only in January, during the cold weather period dominated by high pressure, the delayed break of inversion in the vicinity of Lake Vesijärvi caused the extreme temperature difference to exist in the afternoon, reflecting for its part the substantial stabilising impact of seasonal ice cover on Lake Vesijärvi.

1. Introduction

Spatial temperature differences have been studied with various time scales extending from momentary situations to long-term average conditions. The role of site-specific human-modified or natural environmental factors (e.g. land use, topography, nearby water bodies) affecting spatial temperature differences in a given area can have large seasonal and diurnal variation (e.g. Eliasson and Svensson, 2003; Kolokotroni and Giridharan, 2008; Giridharan and Kolokotroni, 2009). In addition to site-specific characteristics, weather has a remarkable impact on spatial temperature differences, temperature differences being principally largest during calm and clear weather (e.g. Klysik and Fortuniak, 1999; Erell et al., 2011). Consequently, the pre-conditions for large momentary temperature differences cover a wide range of situations.

As for the magnitude of various environment- and weather-driven local temperature differences, urban heat island (UHI) intensity can be over 10 °C (Oke, 1987; Wienert and Kuttler, 2005). Local winds near water bodies have been reported to generate spatial temperature differences of similar magnitude between coastal and inland areas (Kuwagata et al., 1994). In hilly or mountainous areas, topography-enhanced inversions and related cold air pooling can cause temperature differences of over 15 °C within short distances (Pepin et al., 2009). In reality, spatial temperature differences can seldom be comprehensively defined to be caused by a single affecting factor only, but there are many of those involved.

The impact of environmental factors on temperatures has been estimated with various statistical methods, especially with different regression techniques (Hart and Sailor, 2009; Yokobori and Ohta, 2009; Ivajnšič et al., 2014). Development of remote sensing methods and better availability of geographic information system (GIS) datasets have increased GIS-based local climate research during last decades (e.g. Roth et al., 1989; Chapman and Thornes, 2003; Peeters, 2016). Compared to more sophisticated physical models, GIS based methods have proved to be cost-effective options to analyse and represent urban climate as a spatially continuous phenomenon (Szymanowski and Kryza, 2012; Heusinkveld et al., 2014), thus lowering the threshold to utilise local climate data in urban planning (Walther and Olonscheck, 2016). Compared to pure geometric spatialisation algorithms, such as inverse

E-mail addresses: juuso.suomi@utu.fi, juusuo@utu.fi.

https://doi.org/10.1016/j.wace.2017.12.001
Received 13 June 2017; Received in revised form 20 November 2017; Accepted 1 December 2017
Available online 8 December 2017

distance weighting (IDW), regularized spline with tension (RST) and ordinary kriging (OR), the methods that take account of the environmental factors around the observation points, often give more realistic spatially continuous temperature surfaces. The difference is highlighted in study areas with sparse or spatially uneven observation network and large spatial variability in land use, topography, vegetation and other relevant temperature modifying environmental factors. Temporally, the methodological difference is emphasised, when spatial temperature differences are large, e.g. during inversions or strong UHIs (Szymanowski and Kryza, 2009; Hjort et al., 2016; Aalto et al., 2017; Hsu et al., 2017). Many cities still have only few weather observation sites in their area and immediate neighbourhood, which sets a high challenge and demand for the development of sophisticated and cost-effective methods to produce spatially continuous temperature maps from point observation data to be utilised in versatile aspects of city planning (Liu et al., 2017; Sillmann et al., in press).

The extreme events of spatial temperature differences are relevant particularly from a health perspective and connected urban planning viewpoint. Strong UHIs worsen summer-time heat stress in urban areas. As an UHI is typically most pronounced during calm weather when atmospheric mixing is weak, its negative health impacts are often enhanced by poor air quality. Higher urban temperatures also promote the formation of secondary pollutants such as ozone (O_3) (Solecki et al., 2004). Regarding topography, inversions and connected poor atmospheric mixing also remarkably increase the probability of health-risky air quality events especially in cities that are located in valleys (e.g. Baumbach and Vogt, 1999; Wallace et al., 2010; Silcox et al., 2012). During extreme temperature difference situations in winter, slippery conditions can have substantial spatial variation, setting a challenge for road maintenance both in cities and their surroundings (e.g. Gustavsson, 1990; Riehm et al., 2012). The water-body driven local climatic extremes manifest themselves especially in human comfort questions. E.g. in summer, the daytime cooling effect of nearby water bodies can essentially improve thermal comfort in coastal zones (Saaroni and Ziv, 2003).

Better knowledge on the timing, spatial structure, preconditions and environmental drivers of extreme temperature difference situations gives more tools for sustainable urban planning, and supplements the information gained from long-time average temperatures for planning purposes. So far, especially UHI oriented local climate research has been livelier in low latitudes, where heat-related adverse health impacts are a more concrete problem (Wienert and Kuttler, 2005; Gago et al., 2013). As a consequence of climate change, the health perspective is predicted to become more relevant also in high latitudes (Emmanuel and Krüger, 2012; Ward et al., 2016). The warming climate can also alter spatial patterns of winter-time freezing-melting cycles in cool climate regions. For cities to be better prepared, to increase local climate knowledge and to develop its cost effective modelling methods in a changing climate, more information is needed. In this study, extreme temperature difference situations are studied and modelled for the first time in the Lahti region, in order to broaden the scientific basis of relevant city-specific features affecting local climates in high latitudes in particular. The detailed aims of the study are to

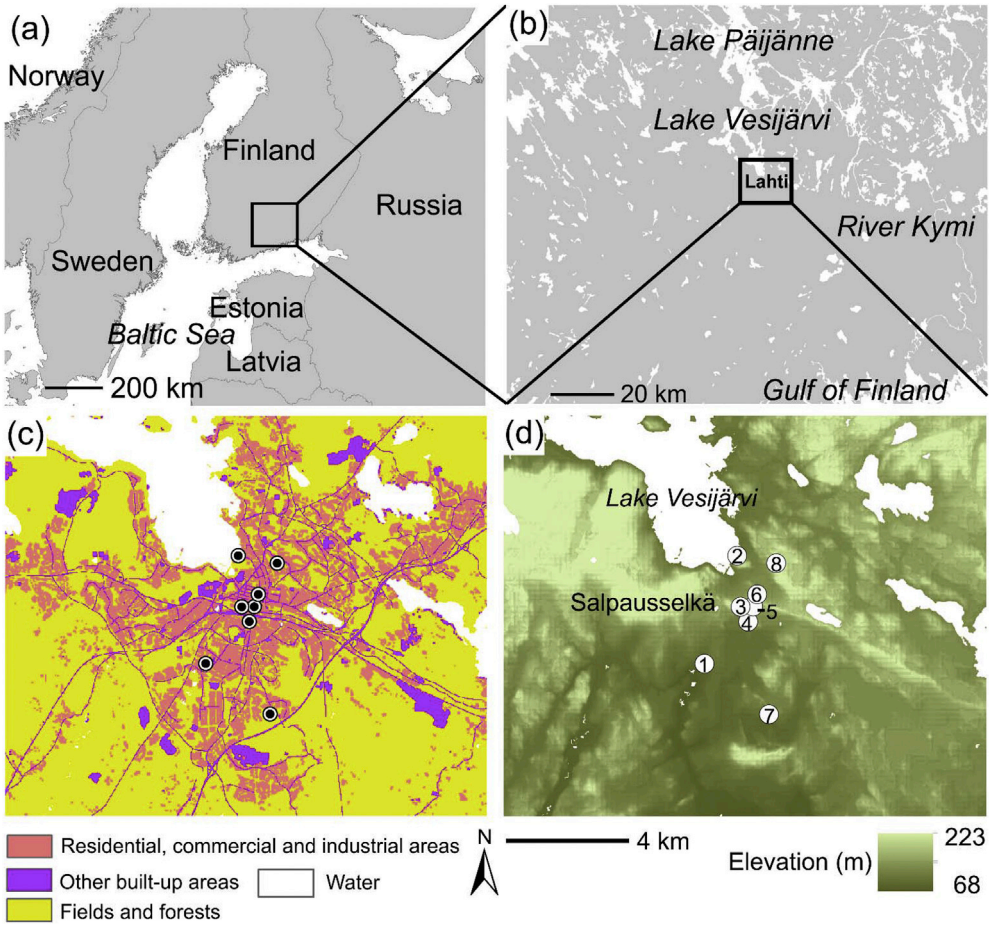

Fig. 1. The study area of Lahti in the southern Finland (a, b). The principal land use (c) and topography (d) with locations of the temperature observation sites. The city centre is in the surroundings of logger site 6. For more information on the logger sites, see Table 1.

1) unravel the seasonal differences in intensity, timing and spatial structure of extreme temperature difference situations in the Lahti region
2) assess the impact of land use, topography and water bodies on temperatures during extreme temperature difference situations
3) explore the role of weather in the manifestation of the extreme temperature difference situations

2. Study area

Lahti is a middle-sized (119 000 inhabitants) city in southern Finland roughly 70 km to the north of the average coastline of the Gulf of Finland (Fig. 1a and b). The total area of Lahti is 517.63 km^2, of which 459.43 km^2 is land and 58.20 km^2 inland waters. During the 30-year period 1981–2010, the annual average temperature in Lahti was 4.5 °C. The coldest month was February and the warmest July, with average temperatures of −7.0 °C and 17.2 °C, respectively. The lowest measured temperature was −35.2 °C (1987) and the highest 35.0 °C (2010). The average annual rainfall was 636 mm. The driest month was typically April (28 mm) and the wettest July (77 mm) (Pirinen et al., 2012). In Köppen's climate classification, Lahti belongs to the hemiboreal and humid Dfb class together with the Baltic countries, Eastern Europe and southern parts of the Scandinavian Peninsula.

Topographically, the Lahti area is characterised by the west-east-oriented glaciofluvial ice marginal deposit Salpausselkä and sporadic hills. Differences in relative elevation are up to 150–160 m inside a 10 km radius around the city centre, located between the Salpausselkä deposit and the largest water body in the region, Lake Vesijärvi (Fig. 1c and d). The core of the city centre (Fig. 1d; Table 1; logger site 6 + surroundings) is bordered by relatively high hills from many compass points. The centre is characterised by a regular grid plan with asphaltised streets and 4 to 8 storey stone houses. The street orientation is roughly from south to north and west to east.

3. Materials and methods

The data used consist of temperature observations, land use data, and topographic data. Temperature data are collected in altogether 8 sites (Fig. 1c and d; Table 1) and with 30 min observation interval by Hobo Pro U23-001 temperature and relative humidity loggers. In this study, the data of the two-year observation period (06/14–05/16) was utilised. The accuracy of the instrument, as claimed by the manufacturer, is ±0.2 °C at 0–50 °C, while the resolution is 0.02 °C. Below 0 °C, the accuracy is slightly worse, being about ±0.38 °C at −20 °C. Loggers are placed inside radiation shields on poles at 3 m elevation above the immediately surrounding ground. Logger elevation deviates from the standard 2-m in order to minimise the risk of vandalism in densely populated areas.

Table 1
Description of the temperature observation sites. For information on the locations of the sites, see Fig. 1.

Site no.	Regional character	Dist. (km) from the market place	Dist. (km) from Lake Vesijärvi[a]	Elevation (m)[b]	Land cover inside the 100 m radius[c]
1	semi-urban	2.74	3.00	76.2	detached houses, roads
2	semi-urban	1.16	0.05	83.6	forest, community service areas
3	rural	0.53	1.20	134.5	sport and recreation areas, park
4	urban	0.95	1.75	91.3	blocks of flats, roads
5	urban	0.47	1.43	109.0	blocks of flats, streets
6	urban	0.24	1.27	99.9	commercial buildings, streets
7	rural	4.05	4.82	85.4	field, forest
8	semi-urban	1.23	1.29	148.0	forest, roads

[a] Shortest distance between shoreline and observation site.
[b] Metres above sea level.
[c] Two most common SLICES land use classes.

The land use and water area calculations were based on SLICES (2010) land use classification with pixel size of 10 m × 10 m. SLICES is a national mapping project founded by the Ministry of Agriculture and Forestry and headed and processed by the National Land Survey of Finland. The classification consists of altogether 45 land use classes including the following eight main classes: A = residential and leisure areas, B = business, administrative, and industrial areas, C = supporting activity areas, D = rock and soil extraction areas, E = agricultural land, F = forestry land, G = other land, and H = water areas. The SLICES classification is suitable for urban climate research, as it is detailed enough to accommodate the spatial differences in both surface characteristics and the amount of anthropogenic heat release. The Digital Elevation Model (DEM) with pixel size of 25 m × 25 m and an elevation resolution of 0.1 m was used in topography calculations. The land use, topography and temperature analyses were conducted with ArcMap, SPSS and MS Excel softwares.

The largest momentary temperature difference situations ($T_{warmest}$-$T_{coldest}$) were sifted on a monthly basis during the two-year (06/14–05/16) period (e.g. largest temperature difference of Junes 2014 and 2015, largest temperature difference of Julys 2014 and 2015 etc.). In order to preliminarily estimate the contribution of environmental factors on temperatures, the situations were typed based on the characters of the warmest and coldest observation sites. Wind speed and cloudiness observations from Finnish Meteorological Institute's observation site in Laune (beside logger site 1 in Fig. 1d) were used to reflect the weather conditions during the extreme situations. To complement the understanding of the seasonal pattern of the incidences of large temperature differences, monthly frequencies of temperature differences exceeding certain threshold values in °C were calculated. Also the 95th and 99th percentiles of the order of magnitude ranked spatial temperature differences ($T_{warmest} - T_{coldest}$) were defined on a monthly basis (see e.g. Sillmann et al., 2013; Easterling et al., 2016).

The more detailed impact of environmental factors on spatial temperature differences was estimated with a stepwise multiple linear regression model including explanatory variables for land use, topography and nearby water areas. The selection of variables was based on expected thermal impacts of environmental factors, earlier experiences in Turku (see e.g. Hjort et al., 2011; Suomi and Käyhkö, 2012; Suomi et al., 2012; Väyrynen et al., 2017), and Pearson's correlation coefficients between the variables and temperatures during the study period.

The impact of land use on temperature was estimated with the SLICES land use classification based 'urban land use' variable, formulated by merging the four original SLICES classes: blocks of flats, office buildings, public buildings, road traffic areas. The area of the new, reclassified 'urban land use' class inside the buffer divided by the total area of the buffer represented the numerical value of the 'urban land use' variable. Buffer sizes of 100 m, 200 m, 300 m and 500 m in radius were tested, beginning from the smallest one, and the buffer size with the highest Pearson's correlation coefficient or clear levelling off in the correlation coefficient between the variable and temperature was selected as the variable quantifying the impact of land use. In addition to the variable as such, also the square root transformations of it were tested with the same principle. The optimal buffer size was determined for each modelled case separately.

The variable reflecting the impact of topography was sifted with the correlation analysis from the potential variables consisting either of buffer based mean elevation or relative elevation. The variables were tested with buffer sizes of 100 m, 200 m, 300 m and 500 m in radius. In case of mean elevation, also the square root transformation of the variable was tested. The mean elevation was formulated by calculating the

average elevation of the circular buffer with a logger site as a central point. The relative elevation was calculated by subtracting the average elevation of the buffer from the elevation of the logger site.

In selecting a variable to represent the thermal impact of water bodies a buffer size of 2 km was applied. Compared to land use and topography, the larger buffer size is justifiable due to the heat storage in a thick layer. Also the relatively large area of Lake Vesijärvi, the locations of the observation sites in relation to the water bodies, and earlier experiences in Turku (Suomi et al., 2012) support the use of a large buffer size. Based on correlation coefficients, either the proportion of water cover inside a 2-km buffer or the square root transformation of the variable was used as an explanatory variable reflecting the impact of water bodies.

After the selection of explanatory variables, stepwise multiple linear regression was performed for each of the momentary extreme situations and for average temperatures of monthly percentiles of 95–100% and 99–100% in order to estimate the thermal impact and relative importance of land use, topography and water bodies on temperatures during different seasons. The stepping method criterion allowed the variables with a statistical significance level of $p \leq 0.05$ to be included in the model.

4. Results

4.1. Momentary extreme situations, frequencies and percentiles

The largest momentary temperature differences varied from

Table 2
Largest temperature difference situations by month with warmest and coldest sites identified. Wind speed and cloudiness observations are from FMI's observation site in Laune (beside the University of Turku's Laune temperature observation site). 'Type of situation' is defined subjectively and is based on the warmness order of the temperature measurement sites. The largest weight is given to the characteristics of the warmest and coldest observation sites.

Max. diff. °C	Date and time (UTC + 2 h)	Warmest site	Temp. °C	Coldest site	Temp. °C	Type of situation	Wind speed (m/s)	Cloudiness, octas
10.1	Fri 22.1.2016, 13:30	Kivistönmäki	−18	Harbour	−28.1	Inversion	0	1
11.1	Mon 16.2.2015, 8:30	Kivistönmäki	−10.2	Laune	−21.3	Inversion	0	0
10.5	Mon 16.3.2015, 0:30	Kivistönmäki	4.3	Laune	−6.2	Inversion	0	0
6.2	Sun 10.4.2016, 23:30	Kivistönmäki	4.2	Laune	−2	Inversion	0	0
9.6	Fri 6.5.2016, 0:00	Kivistönmäki	14.8	Laune	5.2	Inversion	0	0
8.5	Sat 6.6.2015, 1:30	City centre, N[a]	10.8	Laune	2.3	UHI	0	0
7.1	Mon 28.7.2014, 4:00	Kivistönmäki	21.9	Nikkilä	14.8	Inversion	0	5
9.4	Sun 23.8.2015, 4:30	City centre, S[b]	14.6	Laune	5.2	UHI	0	0
8.7	Sat 12.9.2015, 5:30	City centre, S	11	Laune	2.3	UHI	0	0
9	Fri 16.10.2015, 4:30	Harbour	4.7	Laune	−4.3	WLE[c]	0	7
6.8	Tue 24.11.2015, 7:00	Kivistönmäki	−3.4	Laune	−10.2	Inversion	0	1
7.9	Sat 27.12.2014, 6:30	Harbour	−8.4	Laune	−16.3	WLE[c]	0	5

[a] The junction of Aleksanterinkatu and Vesijärvenkatu.
[b] Western side of Vesijärvenkatu, between Puistokatu and Loviisankatu.
[c] Warm lake effect.

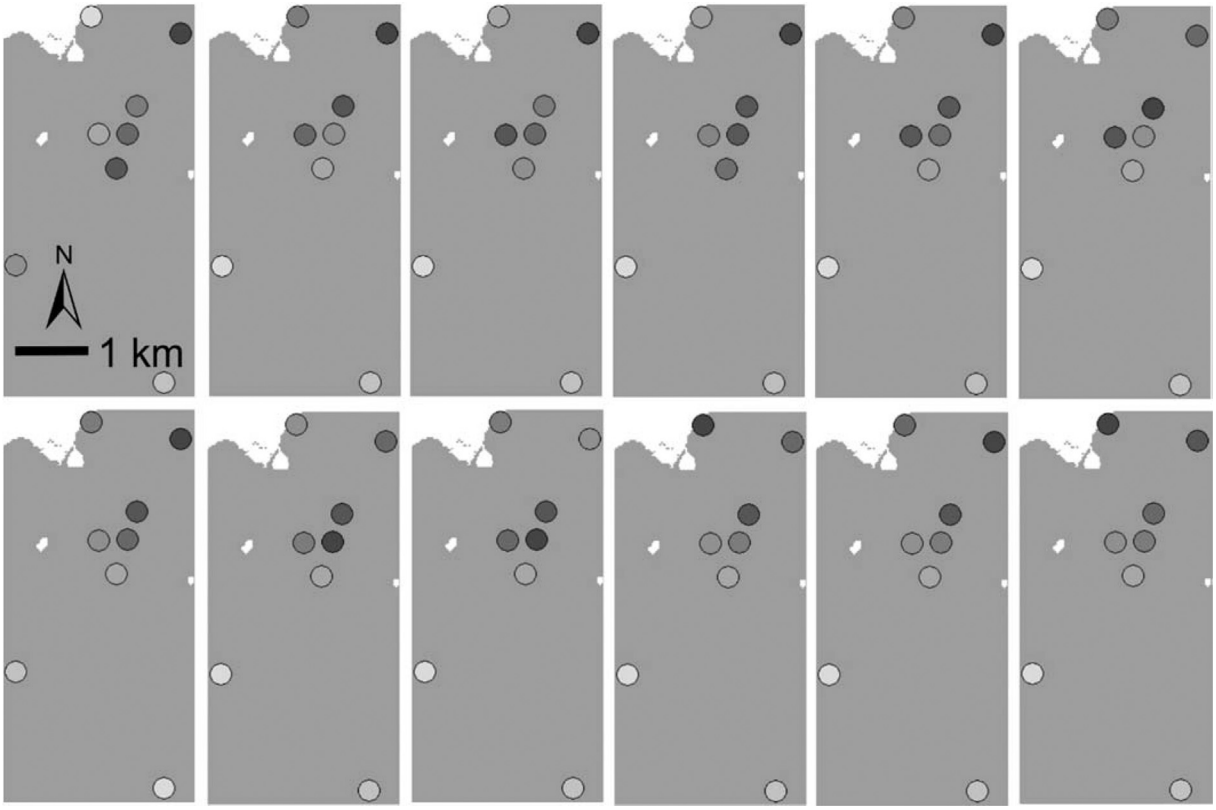

Fig. 2. Warmness order of the observation sites during month-specific extreme situations. Upper row chronologically from left to right: Jan–Jun, lower row respectively: Jul–Dec. The darkest grey denotes the warmest site and lightest grey the coldest, respectively. For further information on the observation sites, see Fig. 1 and Table 1. For information on the timing of the extreme situations, see Table 2.

Table 3
Month-specific frequencies with spatial temperature ranges of a certain magnitudes in 06/14–05/16. The observation interval is 30 min, resulting in total monthly N's of 2736 (Feb), 2880 (Apr, Jun, Sep, Nov) or 2976 (Jan, Mar, May, Jul, Aug, Oct, Dec).

Range (R.)/Month	Jan	Feb	Mar	Apr	May	Jun	Jul	Aug	Sep	Oct	Nov	Dec
6 °C ≤ R. < 8 °C	53	21	136	4	174	37	71	220	206	194	10	28
8 °C ≤ R. <10 °C	9	22	45	0	50	2	0	87	21	13	0	0
R. ≥ 10 °C	1	12	2	0	0	0	0	0	0	0	0	0

Table 4
Monthly 95th and 99th percentiles of order of magnitude ranked spatial temperature differences ($T_{warmest}$–$T_{coldest}$).

PCTL/Mth	Jan	Feb	Mar	Apr	May	Jun	Jul	Aug	Sep	Oct	Nov	Dec
≥99%	7.0	9.0	8.3	5.2	8.3	6.2	6.4	8.7	7.9	7.7	4.8	6.0
≥95%	5.0	3.6	6.5	4.0	6.6	4.5	5.6	7.5	6.5	6.3	1.9	3.7

February's 11.1 °C to April's 6.2 °C (Table 2). Based on the characteristics of the warmest and coldest observation sites, of all the 12 monthly extreme temperature situations, 7 resulted from inversion, with the hill-top site Kivistönmäki (Fig. 1 and Table 1, site 8) as the warmest. Three of the situations were characterised by UHI, and in two of the situations, the excess heat from Lake Vesijärvi caused the harbour to be the warmest area (Table 2; Fig. 2). The coldest site was the detached house area Laune (Fig. 1 and Table 1, site 1) except for January and July. In January the harbour (Fig. 1 and Table 1, site 2) and in July the rural patch in the detached house area in Nikkilä (Fig. 1 and Table 1, site 7) were the coldest. All the extreme situations were characterised by calm weather. During the majority of the situations, the sky was cloudless. The maximum cloud cover, 7/8, was detected during the extreme situation of October. The extreme temperature difference occurred mainly at night or in early morning. Only in January, the extreme situation existed in the afternoon. Concerning days of the week, the extreme situation occurred three times on Mondays and three times on Saturdays, but clear concentration on any certain day was not observed (Table 2).

The frequencies of cases with range of spatial temperature difference ($T_{warmest} - T_{coldest}$) of certain magnitude in °C also had seasonal variation. Temperature differences of 6–8 °C and 8–10 °C were most common in August, whereas temperature differences of 10 °C or more occurred only in January, February and March, with peak of 12 situations in February (Table 3).

Of the 95th and 99th percentiles of ranked temperature differences (Table 4) the 95th percentile followed the same seasonal pattern as the frequencies of 6–10 °C in Table 3, as August had the highest temperature difference threshold of 7.5 °C. The seasonal pattern of 99th percentile, on the contrary, resembles more that of momentary extreme situations, as February had the highest temperature difference of 9.0 °C as a threshold value (Table 4).

4.2. Optimal buffer sizes

The selection of optimal environmental variables applied in the linear regression model was based on a case-specific correlation analysis. Of the tested buffer sizes (100 m, 200 m, 300 m, 500 m in radius) of urban land use variable, the 500 m radius buffer with square root transformation had the highest Pearson's correlation coefficient with the temperatures during the majority of the momentary extreme situations and in all monthly average temperatures of 95^{th}-100^{th} and 99^{th}-100^{th} spatial temperature difference percentiles (Table 5). Concerning topography, the mean elevation of 500 m radius buffer with square root transformation performed best during the momentary situations and percentiles. In the water variable optimization, the square root of water cover area inside 2000 m radius buffer performed best in the majority of situations. Only in January momentary extreme situation and average temperature of 99^{th}-100^{th} percentile did the water cover inside the 2000 m buffer (instead of the square root of that) have a higher correlation coefficient.

4.3. Linear regression models

The results of the linear regression model of the momentary extreme situations support the topography-dominance conclusions made based on the warmest-coldest site comparison, as the topographic variable is included in the regression model in 9 out of 12 of the situations (Table 6). Each time, the direction of the impact is a warming one, i.e. a relatively high position denotes warmer temperatures, reflecting stable atmospheric stratification. The water body variable is included in the model in seven months, whereas the urban variable only twice. The direction of the impact of the water body variable was twofold. In 6 cases out of 7, the impact was a warming one, but in January, the impact was clearly a cooling one. During those two times when the urban variable was included in the model, the impact was a warming one. The explanatory power of the regression model was strongest (adj. $R^2 = 1.00$) in March and weakest (adj. $R^2 = 0.45$) in December. The root mean square error (RMSE) varied accordingly between 0.22 °C and 1.76 °C.

The beta coefficients of linear regression models of 95th – 100^{th} and 99th - 100^{th} percentiles indicate the dominance of topography from December to March, whereas from May to September the urban effect dominates (Table 7). In April and November, the topographic variable is strongest in the 99th – 100^{th} percentile, and the urban variable in the 95th – 100^{th} percentile. The water variable is included in the percentile models 15 times out of 24, but is the strongest variable only in the 99^{th}-100^{th} percentile of October. In the 95th – 100^{th} percentile of October, the impact of topography is the strongest. In monthly percentile models, the beta coefficients were each time positive, indicating a warming impact of urban land use and water bodies, and warmness of high-positioned sites in relation to low-lying areas. The explanatory power of the regression models of percentiles was strongest (adj. $R^2 = 0.98$) in the 99th – 100^{th} percentiles of March and weakest (adj. $R^2 = 0.55$) in the 99th – 100^{th} percentiles of November. The RMSE varied between 0.31 °C and 1.09 °C, respectively.

5. Discussion

The largest momentary temperature difference situations, 95th and 99th percentiles of the temperature differences and frequencies over certain threshold values of temperature differences in °C were studied on a monthly basis in the city of Lahti and its surroundings in southern Finland. The results reveal up to 11 °C spatial temperature differences in the area. Seasonally, the momentary temperature differences were largest in winter, with the peak, 11.1 °C, in February. The majority of the extreme situations, including all three with over 10 °C difference, were characterised by inversions, and consequently, topography was generally the most important environmental factor affecting spatial temperature differences on a short time scale. When moving towards 99th and 95th percentiles and lower temperature difference thresholds in °C, the seasonal peak shifted from winter to August. At the same time, the relevance of urban land use grew and that of topography diminished.

Table 5
Optimal environmental urban topographic and water cover variables and their Pearson's correlation coefficients with temperatures of month-specific momentary extreme situations and month-specific percentiles. The variables were selected to the linear regression model explaining the temperature differences. * = correlation is statistically significant at level $p \leq 0.05$, ** = correlation is statistically significant at level $p \leq 0.01$.

Case/percentile	Urb. var.	Pearson's r	Top. var.	Pearson's r	Water var.	Pearson's r
Fri 22.1.2016, 13:30	500[a]	,388	Re100[b]	,467	Wa	-,878**
Mon 16.2.2015, 8:30	S500[c]	,715*	SAe500[d]	,865**	SWa	,696
Mon 16.3.2015, 0:30	S500	,644	SAe300	,998**	SWa	,275
Sun 10.4.2016, 23:30	S500	,845**	SAe500	,919**	SWa	,378
Fri 6.5.2016, 0:00	S500	,746*	SAe500	,908**	SWa	,600
Sat 6.6.2015, 1:30	S500	,824*	SAe500	,782*	SWa	,624
Mon 28.7.2014, 4:00	S500	,751*	SAe500	,867**	SWa	,643
Sun 23.8.2015, 4:30	S500	,805*	SAe500	,821*	SWa	,663
Sat 12.9.2015, 5:30	S500	,854**	SAe500	,723*	SWa	,592
Fri 16.10.2015, 4:30	S500	,555	SAe500	,611	SWa	,871**
Tue 24.11.2015, 7:00	S500	,633	SAe500	,850**	SWa	,618
Sat 27.12.2014, 6:30	S500	,649	SAe500	,726*	SWa	,656
Jan 99th-100th	S500	,773*	Ae500	,956**	Wa	-,156
Jan 95th-100th	S500	,848**	SAe500	,939**	SWa	,413
Feb 99th-100th	S500	,726*	SAe500	,863**	SWa	,626
Feb 95th-100th	S500	,766*	SAe500	,835**	SWa	,495
Mar 99th-100th	S500	,715*	SAe500	,979**	SWa	,429
Mar 95th-100th	S500	,793*	SAe500	,956**	SWa	,446
Apr 99th-100th	S500	,837**	SAe500	,893**	SWa	,488
Apr 95th-100th	S500	,861**	SAe500	,799*	SWa	,489
May 99th-100th	S500	,824*	SAe500	,770*	SWa	,663
May 95th-100th	S500	,822*	SAe500	,785*	SWa	,658
Jun 99th-100th	S500	,757*	SAe500	,724*	SWa	,725*
Jun 95th-100th	S500	,805*	SAe500	,711*	SWa	,667
Jul 99th-100th	S500	,909**	SAe500	,747*	SWa	,548
Jul 95th-100th	S500	,890**	SAe500	,730*	SWa	,581
Aug 99th-100th	S500	,802*	SAe500	,750*	SWa	,698
Aug 95th-100th	S500	,828*	SAe500	,751*	SWa	,655
Sep 99th-100th	S500	,812*	SAe500	,800*	SWa	,672
Sep 95th-100th	S500	,807*	SAe500	,801*	SWa	,678
Oct 99th-100th	S500	,654	SAe500	,682	SWa	,816*
Oct 95th-100th	S500	,711*	SAe500	,757*	SWa	,744*
Nov 99th-100th	S500	,707*	SAe500	,785*	SWa	,647
Nov 95th-100th	S500	,808*	SAe500	,690	SWa	,599
Dec 99th-100th	S500	,695	SAe500	,735*	SWa	,714*
Dec 95th-100th	S500	,771*	SAe500	,779*	SWa	,684

[a] Optimal buffer size radius in meters.
[b] 'Re' denotes relative elevation.
[c] 'S' denotes square root transformation.
[d] 'Ae' denotes average elevation.

Analogous results indicating the largest momentary temperature differences to occur in winter have been detected in local climate studies e.g. in Łódź, Poland (Klysik and Fortuniak, 1999) and Volos, Greece (Papanastasiou and Kittas, 2012). Short days, weak solar radiation and snow cover favour inversions in winter, and as inversions have been reported to cause larger short term temperature differences than UHIs, the occurrence of largest momentary temperature differences in Lahti in winter is logical (cf. Goldreich, 1984; Brandsma and Wolters, 2012; Pike

Table 6
Results of the linear regression models of the largest momentary temperature difference situations.

Case/percentile	Adjusted R^2	RMSE	Beta coefficients		
			Urban	Topographic	Water
Fri 22.1.2016, 13:30	0.73	1.48			−0.88
Mon 16.2.2015, 8:30	0.97	0.55		0.73	0.50
Mon 16.3.2015, 0:30	1.00	0.22		1.00	
Sun 10.4.2016, 23:30	0.82	0.81		0.92	
Fri 6.5.2016, 0:00	0.94	0.62		0.80	0.38
Sat 6.6.2015, 1:30	0.63	1.55	0.82		
Mon 28.7.2014, 4:00	0.90	0.60		0.75	0.44
Sun 23.8.2015, 4:30	0.84	1.21		0.69	0.48
Sat 12.9.2015, 5:30	0.68	1.64	0.85		
Fri 16.10.2015, 4:30	0.88	0.86		0.41	0.76
Tue 24.11.2015, 7:00	0.84	0.68		0.74	0.42
Sat 27.12.2014, 6:30	0.45	1.76		0.73	

Table 7
Results of the linear regression models of the monthly percentiles.

Percentile	Adjusted R^2	RMSE	Beta coefficients		
			Urban	Topographic	Water
Jan 99th-100th	0.90	0.60		0.96	
Jan 95th-100th	0.94	0.36	0.38	0.68	
Feb 99th-100th	0.88	0.95		0.75	0.42
Feb 95th-100th	0.65	0.93		0.83	
Mar 99th-100th	0.98	0.31		0.93	0.18
Mar 95th-100th	0.90	0.69		0.96	
Apr 99th-100th	0.76	0.80		0.89	
Apr 95th-100th	0.70	0.67	0.86		
May 99th-100th	0.84	1.04	0.69		0.47
May 95th-100th	0.83	0.92	0.69		0.47
Jun 99th-100th	0.81	0.84	0.60		0.56
Jun 95th-100th	0.86	0.66	0.67		0.48
Jul 99th-100th	0.80	0.97	0.91		
Jul 95th-100th	0.88	0.62	0.79		0.37
Aug 99th-100th	0.85	1.06	0.66		0.52
Aug 95th-100th	0.84	0.97	0.70		0.46
Sep 99th-100th	0.83	0.97	0.68		0.49
Sep 95th-100th	0.83	0.87	0.67		0.49
Oct 99th-100th	0.85	0.86		0.50	0.68
Oct 95th-100th	0.84	0.77		0.60	0.58
Nov 99th-100th	0.55	1.09		0.79	
Nov 95th-100th	0.59	0.51	0.81		
Dec 99th-100th	0.76	0.95		0.59	0.56
Dec 95th-100th	0.79	0.59		0.64	0.51

et al., 2013). While the inversion-induced large temperature differences resulted mostly from the strong cooling effect of relatively low-lying areas, the extreme situations in summer, autumn and early winter were mostly due to the warming effect of either urban land use or the relatively warm Lake Vesijärvi. Also then, the outradiation and cooling of topographic lows enhanced the spatial temperature differences. During winter months' inversion-driven extreme situations, the role of the warming factor, i.e. that of the urban land use, was, however, also remarkable, but only in a spatially limited area in the city centre, suppressing inversion there and thus increasing the temperature difference between the city centre and low-lying areas in the surroundings, where inversion kept strong. Ketterer and Matzarakis (2014) stated in their study in Stuttgart, Germany, that complex topography allows the formation of many local climates within a small distance. The phenomenon seems to materialise also in Lahti. Similarly to the observations of Klysik and Fortuniak (1999) in Łódź, Poland and Magee et al. (1999) in Fairbanks, Alaska, the combination of inversion and urban effect seems to generate most favourable pre-conditions for large winter-time temperature differences also in Lahti, although the relatively low-lying city centre partly moderates the impact, causing the semi-urban hill-top site to be the warmest instead of the more urban city centre, indicating dominant impact of topography over that of urban morphology.

Although there was no clear concentration towards any day of the week in the occurrence of momentary extreme situations, all the UHI-driven situations existed during weekend, the fact that can be partly due to the higher human night-time activity and consequently larger anthropogenic heat release in the city centre compared to the situation during weekdays (Allen et al., 2011; Quah and Roth, 2012; Earl et al., 2016).

The extreme situation of January was a good example of the thermal role of ice cover in local climates of high-latitude areas. While during the extreme situations of October and December, the warming effect of Lake Vesijärvi resulted in the harbour being the warmest site, during the January extreme situation, in contrast, the harbour was the coldest site. This extreme situation was preceded by four weeks of continuous frost, and Lake Vesijärvi was ice-covered with no detectable heat excess in the harbour. Along with the formation of ice cover in winter, the low-lying harbour turns from a relatively warm area into a site prone to cold-air drainage and inversions (cf. Overland and Guest, 1991; Pavelsky et al., 2011). A similar continentalising effect of ice cover with increased proneness to coastal zone inversions and related shift of the warmest areas towards the more inland located city centre has also been observed in the Baltic Sea coastal town of Turku, SW Finland (Hjort et al., 2016).

The linear regression model managed to successfully explain the impacts of environmental factors during the momentary extreme situations and 95th -100th and 99th-100th percentiles. The model performance was best in March, when the impact of topography was apparent. The inversion prevailed also in the city centre and harbour, i.e. the impacts of urban land use and the ice-covered Lake Vesijärvi were practically non-existent. A similar seasonal pattern in model performance with the highest explanatory power in March has earlier been detected also in Turku (Suomi and Käyhkö, 2012; Suomi et al., 2012). Similarly to Lahti, the impact of water bodies was, mostly due to the ice cover, minor or non-existent. Based on the results in these topographically different coastal towns, the natural elimination of one of the many affecting factors, with potentially opposite effects, seems to improve the model performance in general. In Lahti, the average elevation based variable performed better than relative elevation, which has proved to be more appropriate in Turku (Hjort et al., 2016; Väyrynen et al., 2017). Differences between these areas indicate that elevation/altitude is principally a valid variable in areas where topographic variation in metres is substantial, but the large-scale elevation does not rise regularly towards any compass point. In areas where this kind of regular rise happens, and differences in small-scale topography are frequent but moderate in metres, relative elevation can better capture the sites prone to cold air drainage (cf. Alcoforado and Andrade, 2006; Ivajnšič et al., 2014; Aalto et al., 2017). Weather, especially atmospheric stratification, also affects the applicability of a variable, and depending on the conditions, either altitude or relative elevation can be more suitable within the same area. In general, the feasibility of pure altitude improves towards windier and cloudier weather, when the impact of other factors is minor (Bogren et al., 2000; Eliasson and Svensson, 2003; Suomi, 2014).

Each extreme situation was characterised by calm weather. In the majority of situations, the sky was clear. The observations on these essential weather parameters are in line with earlier findings reporting negative correlation between spatial temperature differences and cloudiness/wind speed (e.g. Zhang et al., 2010; Ganbat et al., 2013). The mixing of air during windy conditions effectively diminishes local temperature differences, whereas clouds prevent night-time radiative cooling thus reducing probability of large spatial temperature differences caused by inversions and UHIs (Magee et al., 1999; Hinkel et al., 2003). Earlier, results stressing the role of either wind speed (e.g. Ackerman, 1985; Kim and Baik, 2005) or cloudiness (Morris et al., 2001) have been reported. The results of this study support the interpretations that emphasise the more decisive role of wind speed in suppressing spatial temperature differences. Concerning relevant environmental drivers of the extreme situations, during both cases caused by relatively the warm Lake Vesijärvi the cloudiness was substantial (5 and 7 octas), reflecting high moisture content and cloud formation potential of the warm air over the lake and its coastal zone (cf. Kristovich and Steve, 1995; Ackerman et al., 2013). Consequently, large temperature differences caused by relatively warm water bodies tend to be least sensitive to the impact of cloud cover, even if in many cases clouds can be considered a consequence of WLE rather than the independent affecting factor generating pre-conditions for the phenomenon. If the cloudiness is spatially limited and sharp-bordered phenomenon, it can even promote large spatial temperature differences between cloudy and cloudless areas.

Generally, the results of this study indicate that relevant environmental factors affecting spatial temperature differences can be captured rather well with a relatively small number of observation sites, if the sites cover sufficiently different combinations of potential affecting factors. The same national open-source environmental GIS datasets have been successfully utilised, together with remarkably larger temperature observation network, in spatial temperature modelling earlier in another Finnish city, Turku (Hjort et al., 2011, 2016), encouraging the cost-effective broadening of the methodology to other Finnish cities as well. Although there are country-specific differences especially in land use data, the trend towards more easily accessible open-source GIS datasets (GISGeography, 2017) and already existing continental data (e.g. EEA, 2012) support the utilisation of the methodology or parts of it also in the foreign cities.

The inclusion of environmental factors in the spatialisation of point temperature data often improves the accuracy compared to the more general geometric and distance based interpolation methods (Szymanowski and Kryza, 2009). The GIS data based statistical modelling is a cost effective option to sophisticated physical and dynamic urban temperature models, especially when the study area is large or when the temperatures are extrapolated beyond the measurement network (Brandsma and Wolters, 2012; Walther and Olonscheck, 2016). The environmental factors applied in this study have proved to be relevant also in other climatic zones (e.g. Alcoforado and Andrade, 2006; Santamouris, 2015; Morris et al., 2016), but the wide spectrum of variables with various buffer sizes applied in earlier studies both within and between different areas indicate, together with the results of this study, that site-specific, seasonal and weather based considerations are crucial especially in the formulation of variables and selecting their optimal spatial scales (Giridharan et al., 2008; Suomi et al., 2012; van Hove et al., 2015; Hjort et al., 2016).

6. Conclusions

The results of this study indicate that the largest momentary

temperature differences in the high-latitude city of Lahti occur during winter-time inversions, reflecting the dominant role of topography over that of land use and water bodies. In summer, however, the urban heat island causes the largest momentary temperature differences, and in autumn the heating impact of Lake Vesijärvi is crucial. In winter, the ice cover effectively neutralises the lake's climatic impact. When moving from the momentary temperature difference extremes towards 99th and 95th percentiles, the role of urban land use grew and that of topography diminished. A calm weather, i.e. lack of wind, was a necessary prerequisite for large temperature differences in the study area. The role of cloud cover was less critical in suppressing large spatial temperature differences. The linear regression model with open source GIS data based variables managed well to capture the relevant environmental factors affecting spatial temperature differences in the study area.

Acknowledgements

Financial support in the form of personal scholarship for this research was provided by the Tiina and Antti Herlin Foundation. The scholarship enabled data collection and interpretation, data analysis, preparation of the article and decision to submit it for publication. The co-operation with the cities of Lahti and Turku has been very valuable.

References

Aalto, J., Kämäräinen, M., Shodmonov, M., Rajabov, N., Venäläinen, A., 2017. Features of Tajikistan's past and future climate. Int. J. Clim. 37 (14), 4949–4961.
Ackerman, B., 1985. Temporal March of the Chicago heat island. J. Clim. Appl. Meteorol. 24, 547–554.
Ackerman, S.A., Heidinger, A., Foster, M.J., Maddux, B., 2013. Satellite regional cloud climatology over the Great Lakes. Remote Sens. 5, 6223–6240.
Alcoforado, M.J., Andrade, H., 2006. Nocturnal urban heat island in Lisbon (Portugal): main features and modelling attempts. Theor. Appl. Climatol. 84, 151–159.
Allen, L., Lindberg, F., Grimmond, C.S.B., 2011. Global to city scale urban anthropogenic heat flux: model and variability. Int. J. Clim. 31 (13), 1990–2005.
Baumbach, G., Vogt, U., 1999. Experimental determination of the effect of mountain-valley breeze circulation on air pollution in the vicinity of Freiburg. Atmos. Environ. 33 (24–25), 4019–4027.
Bogren, J., Gustavsson, T., Postgård, U., 2000. Local temperature differences in relation to weather parameters. Int. J. Clim. 20, 151–170.
Brandsma, T., Wolters, D., 2012. Measurement and statiscal modeling of the urban heat island of the city of Utrecht (The Netherlands). J. Appl. Meteorol. Clim. 51, 1046–1060.
Chapman, L., Thornes, J.E., 2003. The use of geographical information systems in climatology and meteorology. Progr. Phys. Geogr. 27, 313–330.
Earl, N., Simmonds, I., Tapper, N., 2016. Weekly cycles in peak time temperatures and urban heat island intensity. Environ. Res. Let. 11 (7), 1–10.
Easterling, D.R., Kunkel, K.E., Wehner, M.F., Sun, L., 2016. Detection and attribution of climate extremes in the observed record. Weather Clim. Extrem 11, 17–27.
EEA (European Environment Agency), 2012. CORINE Land Cover. EEA, Denmark.
Eliasson, I., Svensson, M.K., 2003. Spatial air temperature variations and urban land use – a statistical approach. Meteorol. Appl. 10, 135–149.
Emmanuel, R., Krüger, E., 2012. Urban heat island and its impact on climate change resilience in a shrinking city: the case of Glasgow, UK. Build. Environ. 53, 137–149.
Erell, E., Pearlmutter, D., Williamson, T., 2011. Urban Microclimate. Designing the Spaces between Buildings. Earthscan, London, p. 266.
Gago, E.J., Roldan, J., Pacheco-Torres, R., Ordóñez, J., 2013. The city and urban heat islands; A review of strategies to mitigate adverse effects. Renew. Sust. Energy Rev. 25, 749–758.
Ganbat, G., Han, J.-Y., Ryu, Y.-H., Baik, J.-J., 2013. Characteristics of the urban heat island in a high-altitude metropolitan city, Ulaanbaatar, Mongolia. Asia-Pac. J. Atmos. Sci. 49 (4), 535–541.
Giridharan, R., Lau, S.S.Y., Ganesan, S., Givoni, B., 2008. Lowering the outdoor temperature in highrise high-density residential developments of coastal Hong Kong: vegetation influence. Build. Environ. 43, 1583–1595.
Giridharan, R., Kolokotroni, M., 2009. Urban heat island characteristics in London during winter. Sol. Energy 83 (9), 1668–1682.
GISGeography, 2017. http//gisgeography.com. (Accessed 12 June 2017).
Goldreich, Y., 1984. Urban topoclimatology. Prog. Phys. Geogr. 8, 336–364.
Gustavsson, G., 1990. Variation in road surface temperature due to topography and wind. Theor. Appl. Climatol. 41 (4), 227–236.
Hart, M.A., Sailor, D.J., 2009. Quantifying the influence of land-use and surface characteristics on spatial variability in the urban heat island. Theor. Appl. Climatol. 95, 397–406.
Heusinkveld, B.G., Steeneveld, G.J., van Hove, L.W.A., Jacobs, C.M.J., Holtslag, A.M.M., 2014. Spatial variability of the Rotterdam urban heat island as influenced by urban land use. J. Geophys. Res.-Atmos 119, 677–692.
Hjort, J., Suomi, J., Käyhkö, J., 2011. Spatial prediction of urban-rural temperatures using statistical methods. Theor. Appl. Climatol. 106, 139–152.
Hjort, J., Suomi, J., Käyhkö, J., 2016. Extreme urban–rural temperatures in the coastal city of Turku, Finland: quantification and visualization based on a generalized additive model. Sci. Total Environ. 569–570, 507–517.
Hinkel, K.M., Nelson, F.E., Klene, A.E., Bell, J.H., 2003. The urban heat island in winter at Barrow, Alaska. Int. J. Clim. 23, 1889–1905.
Hsu, S., Mavrigianni, A., Hamilton, I., 2017. Comparing spatial interpolation techniques of local urban temperature for heat-related health risk estimation in a subtropical city. Procedia Eng. 198, 354–365.
Ivajnšič, D., Kaligarič, M., Žiberna, I., 2014. Geographically weighted regression of the urban heat island of a small city. Appl. Geogr. 53, 341–353.
Ketterer, C., Matzarakis, A., 2014. Human-biometeorological assessment of the urban heat island in a city with complex topography – the case of Stuttgart, Germany. Urban Clim. 10, 573–584.
Kim, Y.-H., Baik, J.-J., 2005. Spatial and temporal structure of the urban heat island in Seoul. J. Appl. Meteorol. 44 (5), 591–605.
Klysik, K., Fortuniak, K., 1999. Temporal and spatial characteristics of the urban heat island of Lodz. Pol. Atmos. Environ. 33, 3885–3895.
Kolokotroni, M., Giridharan, R., 2008. Urban heat island intensity in London: an investigation of the impact of physical characteristics on changes in outdoor air temperature during summer. Sol. Energy 82 (11), 986–998.
Kristovich, D.A.R., Steve, R.A., 1995. A satellite study of cloud-band frequencies over the Great Lakes. J. Appl. Meteorol. 34 (9), 2083–2090.
Kuwagata, T., Kondo, J., Sumioka, M., 1994. Thermal effect of the sea breeze on the structure of the boundary layer and the heat budget over land. Bound.-Lay. Meteorol. 67 (1), 119–144.
Liu, L., Lin, Y., Liu, J., Wang, L., Wang, D., Shui, T., Chen, X., Wu, Q., 2017. Analysis of local-scale urban heat island characteristics using an integrated method of mobile measurement and GIS-based spatial interpolation. Build. Environ. 117, 191–207.
Magee, N., Curtis, J., Wendler, G., 1999. The urban heat island effect at Fairbanks, Alaska. Theor. Appl. Climatol. 64, 39–47.
Morris, C.J.G., Simmonds, I., Plummer, N., 2001. Quantification of the influences of wind and cloud on the nocturnal urban heat island of a large city. J. Appl. Meteorol. 40, 169–182.
Morris, K.I., Chan, A., Ooi, M.C., Oozeer, M.Y., Abakr, Y.A., Morris, K.J.K., 2016. Effect of vegetation and waterbody on the garden city concept: an evaluation study using a newly developed city, Putrajaya, Malaysia. Comput. Environ. Urban 58, 39–51.
Oke, T.R., 1987. Boundary Layer Climates, second ed. Routledge, London.
Overland, E.O., Guest, P.S., 1991. The Arctic snow and air temperature budget over sea ice during winter. J. Geophys. Res. 96 (C3), 4651–4662.
Papanastasiou, D.K., Kittas, C., 2012. Maximum urban heat island intensity in a medium-sized coastal Mediterranean city. Theor. Appl. Climatol. 107, 407–416.
Pavelsky, T.M., Boé, J., Hall, A., Fetzer, E.J., 2011. Atmospheric inversion strength over polar oceans in winter regulated by sea ice. Clim. Dynam. 36 (5), 945–955.
Peeters, A., 2016. A GIS-based method for modeling urban-climate parameters using automated recognition of shadows cast by buildings. Comput. Environ. Urban 59, 107–115.
Pepin, N.C., Schaefer, M.K., Riddy, L.D., 2009. Quantification of the cold-air pool in Kevo Valley, Finnish Lapland. Weather 64 (3), 60–67.
Pike, G., Pepin, N.C., Schaefer, M., 2013. High latitude local scale temperature complexity: the example of Kevo Valley, Finnish Lapland. Int. J. Clim. 33 (8), 2050–2067.
Pirinen, P., Simola, S., Aalto, J., Kaukoranta, J.-P., Karlsson, P., Ruuhela, R., 2012. Tilastoja Suomen Ilmastosta 1981–2010. In: Raportteja 2012: 1. Finnish Meteorological Institute, , Helsinki. https://helda.helsinki.fi/handle/10138/35880. Accessed 7 December 2016.
Quah, A.K.L., Roth, M., 2012. Diurnal and weekly variation of anthropogenic heat emissions in a tropical city, Singapore. Atmos. Environ. 46, 92–103.
Riehm, M., Gustavsson, T., Bogren, J., Jansson, P.-E., 2012. Ice formation detection on road surfaces using infrared thermometry. Cold Reg. Sci. Technol. 83–84, 71–76.
Roth, M., Oke, T.R., Emery, W.J., 1989. Satellite-derived urban heat island from three coastal cities and the utilization of such data in urban climatology. Int. J. Remote Sens. 10, 1699–1720.
Saaroni, H., Ziv, B., 2003. The impact of a small lake on heat stress in a Mediterranean urban park: the case of Tel Aviv, Israel. Int. J. Biometeorol. 47, 156–165.
Santamouris, M., 2015. Analyzing the heat island magnitude and characteristics in one hundred Asian and Australian cities and regions. Sci. Total Environ. 512–513, 582–598.
Silcox, G.D., Kelly, K.E., Crosman, E.T., Whiteman, C.D., Allen, B.L., 2012. Wintertime PM2.5 concentrations during persistent, multi-day cold-air pools in a mountain valley. Atmos. Environ. 46, 17–24.
Sillmann, J., Kharin, V.V., Xhang, X., Zwiers, F.W., Bronaugh, D., 2013. Climate extremes indices in the CMIP5 multimodel ensemble: Part 1. Model evaluation in the present climate. J. Geophys. Res.-Atmos 118, 1716–1733.
Sillmann, J., Thorarinsdottir, T., Keenlyside, N., Schaller, N., Alexander, L.V., Hegerl, G., Seneviratne, S.I., Vautard, R., Zhang, X., Zwiers, F.W., 2017. Understanding, modeling and predicting weather and climate extremes: challenges and opportunities. Weather Clim. Extrem. https://doi.org/10.1016/j.wace.2017.10.003.
Solecki, W.D., Rosenzweig, C., Pope, G., Chopping, M., Goldberg, R., Polissar, A., 2004. Urban heat island and climate change: an assessment of interacting and possible adaptations in the Camden, New Jersey Region. Environ. Assess. Risk Anal. Elem. Res. Proj. Summ. 5.
Suomi, J., 2014. Characteristics of Urban Heat Island (UHI) in a High-latitude Coastal City - a Case Study of Turku. Department of Geography and Geology, University of Turku, SW Finland, p. 70 (Ph.D. thesis).

Suomi, J., Hjort, J., Käyhkö, J., 2012. Effects of scale on modelling the urban heat island in Turku, SW Finland. Clim. Res. 55, 121–136.
Suomi, J., Käyhkö, J., 2012. The impact of environmental factors on urban temperature variability in the coastal city of Turku. SW Fnl. Int. J. Clim. 32, 451–463.
Szymanowski, M., Kryza, M., 2009. GIS-based techniques for urban heat island spatialization. Clim. Res. 38, 171–187.
Szymanowski, M., Kryza, M., 2012. Local regression models for spatial interpolation of urban heat island - an example from Wrocław, SW Poland. Theor. Appl. Climatol. 108, 53–71.
van Hove, L.W.A., Jacobs, C.M.J., Heusinkveld, B.G., Elbers, J.A., van Driel, B.L., Holtslag, A.A.M., 2015. Temporal and spatial variability of urban heat island and thermal comfort within the Rotterdam agglomeration. Build. Environ. 83, 91–103.
Väyrynen, R., Suomi, J., Käyhkö, J., 2017. Fine-scale analysis of sea effect on coastal air temperatures at different time scales. Boreal Environ. Res. 22, 369–383.
Wallace, J., Corr, D., Kanaroglou, P., 2010. Topographic and spatial impacts of temperature inversions on air quality using mobile air pollution surveys. Sci. Total Environ. 408 (21), 5086–5096.
Walther, C., Olonscheck, M., 2016. Analyzing heat exposure in cities by applying meteorological data from the hinterland. Meteorol. Appl. 23 (3), 541–553.
Ward, K., Lauf, S., Kleinschmit, B., Endlicher, W., 2016. Heat waves and urban heat islands in Europe: a review of relevant drivers. Sci. Total Environ. 569–570, 527–539.
Wienert, U., Kuttler, W., 2005. The dependence of the urban heat island intensity on latitude – a statistical approach. Meteorol. Z. 14 (5), 677–686.
Yokobori, T., Ohta, S., 2009. Effect of land cover on air temperatures involved in the development of an intra-urban heat island. Clim. Res. 39, 61–73.
Zhang, K., Wang, R., Shen, C., Da, L., 2010. Temporal and spatial characteristics of the urban heat island during rapid urbanization in Shanghai, China. Environ. Monit. Assess. 169, 101–112.